ACS OMEGA

Open Access

http://pubs.acs.org/journal/acsodf

Article

Rapid Quantitative Detection for Nitrofurantoin Based on Nitrogen-Doped Highly Photoluminescent Carbon Dots

Xing Zhao,[§] Shiwen Chen,[§] Yangyang Fan, Xianglan Lei, Yulin Li, Tianxing Ji, Hui Xia,* and Lu Wang*

Cite This: *ACS Omega* 2024, 9, 13183−13190

Read Online

ACCESS | Metrics & More | Article Recommendations | Supporting Information

ABSTRACT: Nitrogen-doped carbon dots (NCD) with high fluorescence retention and good stability were successfully fabricated using citric acid and urea via a facile and eco-friendly one-step microwave method, which exhibited superior specificity for detection of nitrofurantoin (NFT). Upon the addition of NFT, the fluorescence intensity of NCD at 450 nm was significantly decreased. Besides, a satisfactory linear relationship between the fluorescence quenching efficiency and concentrations of NFT was obtained. Especially, NCD was qualitatively and quantitatively applied for detection NFT in milk and meat extract samples with a high recovery rate. Consequently, it was suggested that the detection method had potential application in the specific detection of NFT, offering a novel approach for veterinary drug residue detection.

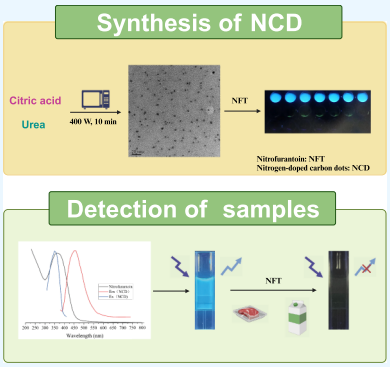

1. INTRODUCTION

Nitrofurans is special kind of antibiotic that play a significant role in the prevention of infections due to inhibiting growth of bacteria.[1,2] In addition, they are often used as an feed additive to promote animal growth in animal husbandry.[3] However, excessive use of antibiotics can lead to antibiotic residues in food and the environment, posing lots of threats to human health, including toxic effects, bacterial resistance to antibiotics, and so on.[4,5] NFT was previously used in veterinary and agricultural settings, but it has been banned.[6] Therefore, this kind of antibiotic detection is of special concern to protect human health and the environment.

Traditional technologies for antibiotics detection include high-performance liquid chromatography,[7] capillary electrophoresis,[8] and liquid chromatography−mass spectrometry.[9,10] Though these methodologies can detect antibiotics in extremely high sensitivity and accuracy, they involve sophisticated and high-cost instrumentation.[11] Besides, they tend to require complex sample preparation, professional instrument operation as well as long analysis times.[12] Thus, it is still a challenge to develop a better analytical method for the qualitative and quantitative determination of antibiotics. Fluorescence analysis are considered as a rapid, facile, real-time, economical, and selective method in the detection field,[13] especially for the processed of bulk samples.[14] The fluorescence method can be wildly used to the detection of antibiotics,[15,16] pesticides,[17,18] and metal ions[19,20] in the environment.[21,22] NFT is a nitro-containing compound that serves as a fluorescence quencher. This is attributed to the presence of the $-NO_2$ moiety, a common electron-withdrawing group with oxidizing properties, capable of attenuating or even quenching fluorescence.[23] Leveraging this characteristic, the fluorescence methodology can be employed for the detection of furanone.

Carbon quantum dots (CD) as novel nanomaterials have attracted remarkable attention for simple and rapid detection due to promising fluorescent properties and superior photostability.[22,24] The photoluminescence of CD was used as the response signal to monitor the presence of antibiotics.[25] Wang's group prepared a kind of CD modified with piperazine.[26] The CD can be used in the detection of oxytetracycline due to the Förster resonance energy transfer (FRET) between the CD and oxytetracycline. The PL intensity and detection process of CD were dependent on the pH. Heteroatom doping of CD can regulate the surface chemical structure to improve the fluorescence intensity. Qi and his co-workers synthesized NCD with excellent photoluminescence properties.[27] The NCD showed high sensitivity and selectivity to tetracycline, aureomycin, and so on. However, the synthesis of NCD based on the hydrothermal method was complicated, time-consuming, and ungreen. Eco-friendly fabrication of CD is especially important for matching with a sustainable environment. Microwave-assisted strategy obtains advantages, including environment-friendly, efficiently, simplicity, and desired morphology.[28]

Received: December 6, 2023
Revised: February 13, 2024
Accepted: February 20, 2024
Published: March 4, 2024

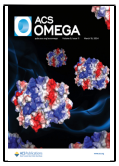

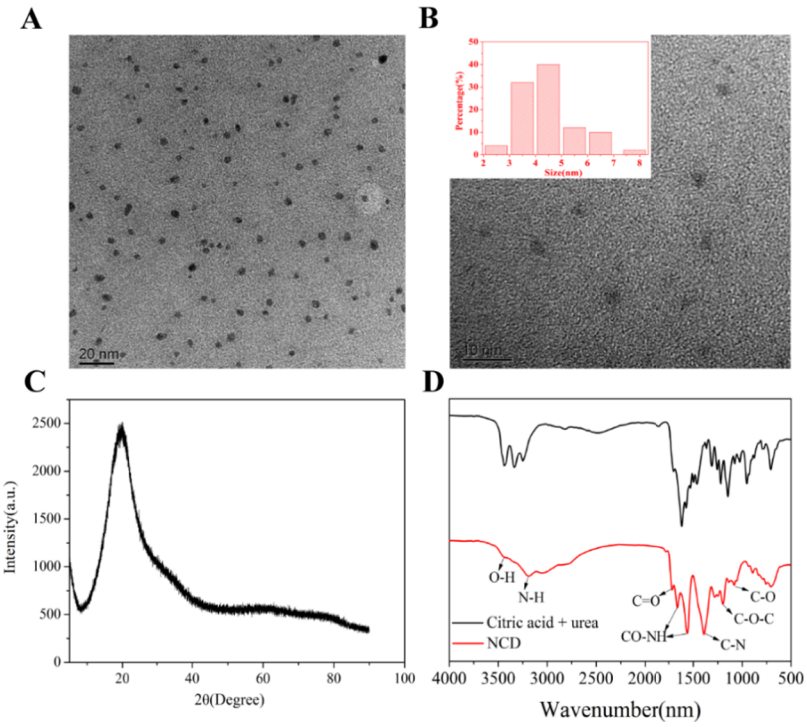

Figure 1. (A) TEM image of the NCD. (B) High-resolution TEM image of NCD (inset shows the diameter distribution of NCD). (C) XRD pattern of NCD. (D) FT-IR spectrum of NCD (red) and mixture of citric acid and urea (black).

In this work, highly efficient fluorescent nitrogen-doped carbon dots (NCD) were fabricated via microwave-assisted synthesis using citric acid and urea.[29] The morphology, structure, and fluorescence properties of NCD were characterized. Subsequently, highly selective and sensitive detection of NFT was investigated by fluorescent quenching. NCD served as fluorescent probe for the visual detection NFT. Importantly, NCD exhibited excellent detection effect in different solution system like milk[30] and meat extract.[31] Consequently, NCD was expected to be a potential demonstration of simple, rapid, visual, and real-time detection of NFT.

2. EXPERIMENTAL SECTION

2.1. Materials. Citric acid and urea were purchased from Kermel Chemical Reagent Co., Ltd. (Tianjin, China); nitrofurantoin (NFT), polymyxin, ampicillin, enrofloxacin, cefpirome, gentamicin, and streptomycin were purchased from Shanghai yuanye Bio-Technology Co., Ltd. Milk, and meat were purchased from supermarket. All of the chemical reagents in this study are of analytical grade and are used without further purification. All aqueous solutions are prepared with deionized water.

2.2. Synthesis of NCD. Citric acid (1 g) and urea (0.5 g) were dissolved in 10 mL of purified water. Then, the mixture was treated in a microwave system at 400 W for 10 min. As the microwave irradiation time increased, the color of the solution turned brown, indicating the formation of NCD and that the resulting products were cooled at room temperature. Then, a small amount of water was added, followed by centrifugation at 10,000 rpm for 10 min. The obtained supernatant was freeze-dried. The brownish yellow powder was NCD. The yield of NCD was 52.86%.

2.3. Characterization of NCD. Transmission electron microscopy (TEM) images were generated by using a Tecnai G2 F20 microscope (FEI, USA). The infrared spectra were recorded on a Nicolet 6700FTIR spectrometer (Thermo Scientific, USA). Absorption spectra was obtained using SpectraMax iD3(Molecular Devices). X-ray photoelectron spectroscopy (XPS) experiments were performed on a 5000 VersaProbe III spectrometer (PHI, Japan). X-ray diffraction (XRD) pattern of NCD was recorded on a D8 Advance (Bruker, German). All fluorescent spectra were performed on a SpectraMax iD3(Molecular Devices). Steady-state/Lifetime Spectrofluorometer (FS 5, Edinburgh Instruments, UK) was used to measure the fluorescence lifetime and quantum yield of NCD.

2.4. NCD Detection of NFT. One mL of NCDs (1 mg/mL, pH 7) and 1 mL of antibiotics solution (NFT) with different concentrations (10.000, 5.000, 2.500, 1.250, and 0.625 mg/mL) were mixed. After reaction at room temperature for 5 min, the mixture solution transferred to a 96-well plate, and the fluorescence intensity (F) was recorded under consistent conditions at an excitation wavelength of 350 nm. The fluorescence intensity without antibiotics (F_0) was tested by the same method. The fluorescence quenching rate was the ratio of the fluorescence intensity before and after adding antibiotics.

2.5. Detection of NFT in Real Samples. Two kinds of samples (milk and meat) were selected for real sample analysis. All samples were centrifuged to remove the solid particles and suspended solids. Then the solution was filtered with a 0.22 μm microporous membrane. Different concentrations of the NFT solution were added to the samples. Finally, the concentration of NFT was determined by the method described above method. The recovery rate was calculated according to the following formula:

$$\text{Recovery rate} = C/C_0 \times 100\%$$

https://doi.org/10.1021/acsomega.3c09620
ACS Omega 2024, 9, 13183−13190

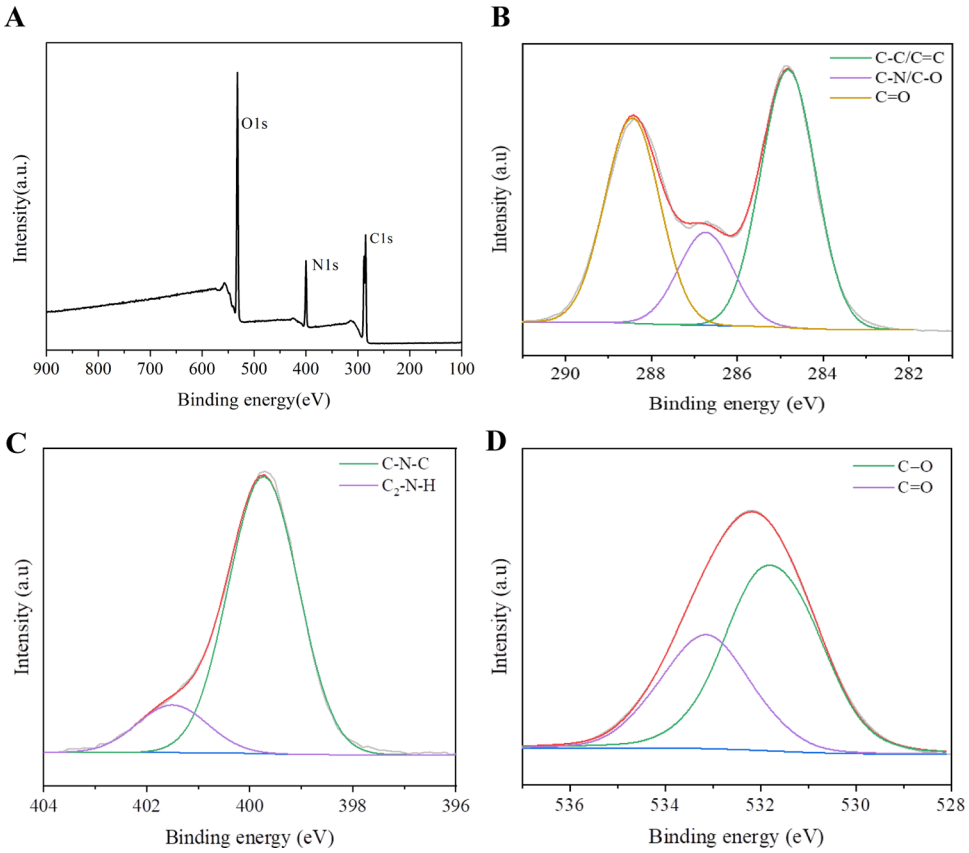

Figure 2. (A) XPS spectra of the NCD. (B) C 1s spectrum and fitting curves. (C) N 1s spectrum and fitting curves. (D) O 1s spectrum and fitting curves.

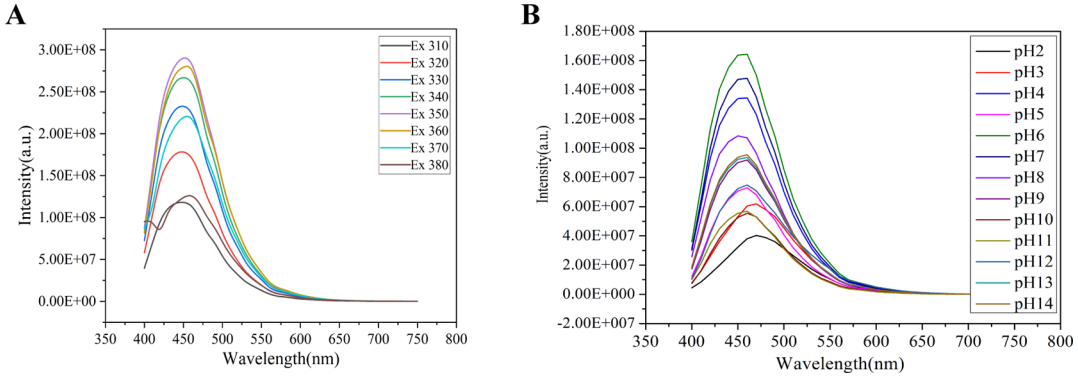

Figure 3. (A) Fluorescence spectra of NCD with different excitation wavelengths (from 310 to 380 nm). (B) Fluorescence spectra of NCD in different pH.

C is the sample concentration measured according to the above method, and C_0 is the known concentration of the addition of the standard.

3. RESULTS AND DISCUSSION

3.1. Structural and Morphology Characterization of NCD. The morphology and size of NCD were characterized by TEM. As shown in Figure 1A,B, the as-prepared NCD had uniform dispersion and displayed spherical particles. The size distribution of NCD calculated by measuring 80 particles indicated that the average diameter was 3−5 nm approximately. The TEM images confirmed that NCD obtained a spherical structure, good dispersity, and uniform size. The XRD pattern of NCD shows that a diffraction peak existed at $2\theta = 19.9°$, which was corresponded to the diffraction peak of the (002) diffraction pattern of graphite carbon (Figure 1C).[32] The result indicated that NCD had a graphite-like structure.

The elemental composition and surface chemical structure were determined by XPS and Fourier transform infrared spectroscopy (FT-IR) (Figure 1D). The XPS spectrum of NCD showed the peaks at 285.08, 400.08, and 532.08 eV in Figure 2A, corresponding to C 1s, N 1s, and O 1s electrons, respectively. The high-resolution spectrum of C 1s shows three peaks at 285, 531.4, and 532.6 eV, representing C−C/C═C, C−N/C−O, and C═O groups (Figure 2B).[33,34] In the high-resolution N 1s spectrum (Figure 2C), the two peaks at 399.71 and 401.50 eV could be assigned to the C−N−C and C_2−N-H functional groups.[32,33,35] The O 1s spectrum shows two fitting

https://doi.org/10.1021/acsomega.3c09620
ACS Omega 2024, 9, 13183−13190

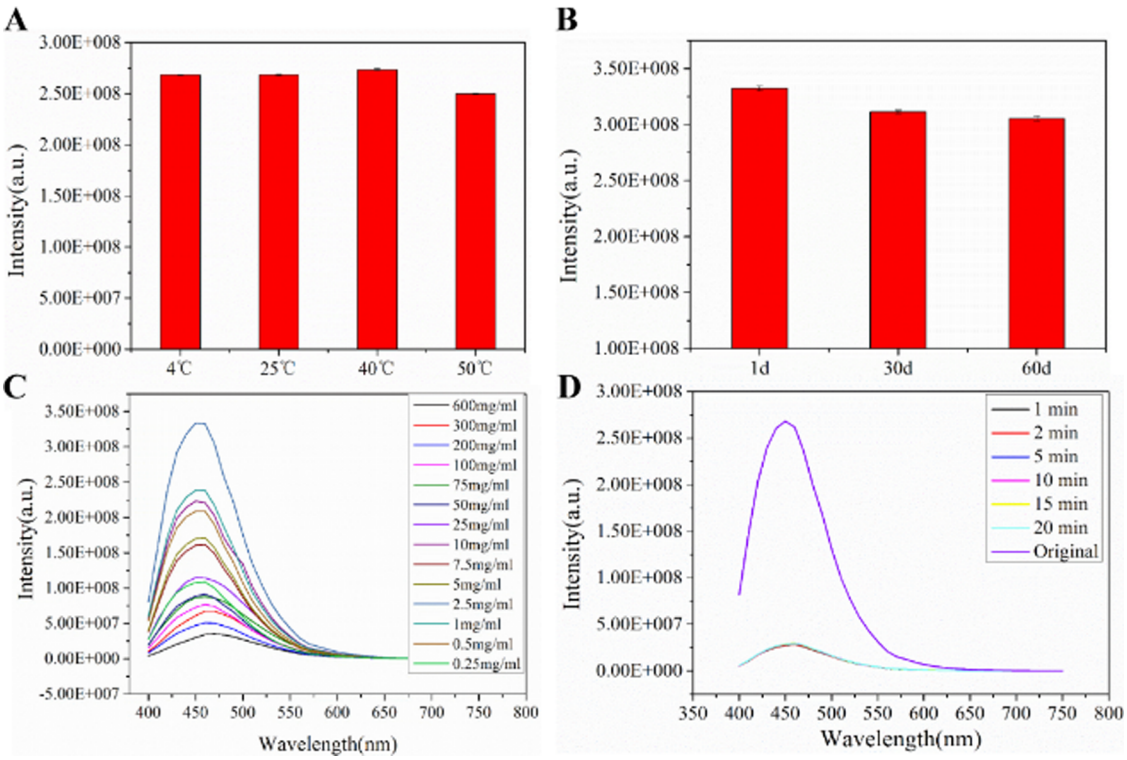

Figure 4. Fluorescence intensity of NCD at various conditions: (A) Temperature. (B) Storage time. (C) NCD concentration. (D) Detection time.

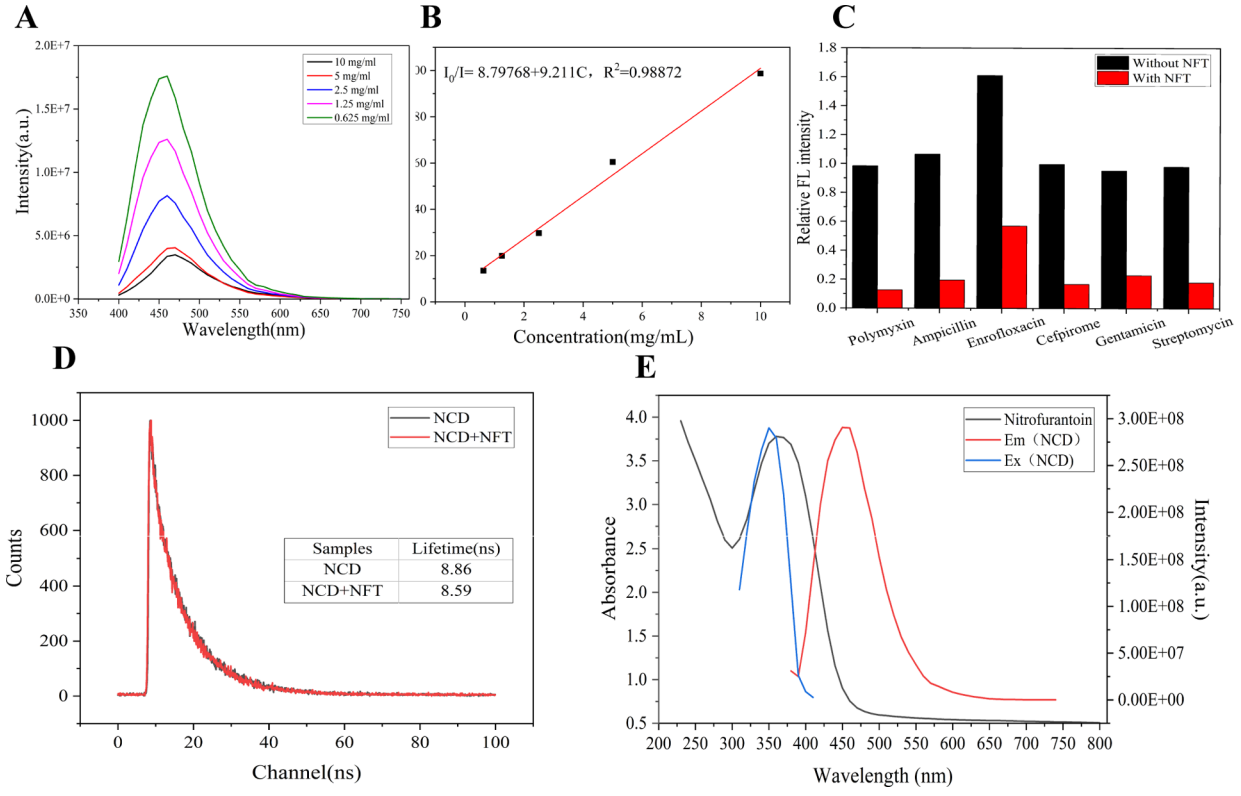

Figure 5. (A) Fluorescence intensity of NCD with different concentrations. (B) Relationship curve between F_0/F and the concentration of NFT. (C) Selectivity of NCD for NFT in the presence of different antibiotics. (D) Fluorescence lifetime. (E) UV−vis absorption spectrum of NFT (black line), the fluorescence spectrum of NCD (blue line, λ_{ex} = 350 nm), and excitation spectrum of NCD (read line, λ_{em} = 450 nm).

peaks at 531.41 and 532.26 eV, belonging to the C−O and C═O groups, respectively (Figure 2D).[36−38] Moreover, the FT-IR spectra were employed to further confirm the existence of the functional groups in Figure 1D. The characteristic peaks at 3185 and 3432 cm^{-1} represented the stretching vibrations of N−H and O−H. The peaks at 1720 cm^{-1} were attributed to

https://doi.org/10.1021/acsomega.3c09620
ACS Omega 2024, 9, 13183−13190

stretching vibrations of C═O. The absorption peak at 1388 cm^{-1} was belonged to the C−N bending vibration. The FT-IR analysis result was consistent with the C 1s, N 1s, and O 1s spectra. The results presented above indicated that NCD were successfully prepared.

3.2. Optical Properties of NCD. Fluorescence quantum yield is a key parameter for assessing the luminescent performance of NCD. According to the results obtained from steady-state/transient fluorometry measurements, the fluorescence quantum yield of the produced NCD in this experiment was determined to be 20.41%. The absorption and fluorescence properties of NCD were explored by UV−vis spectroscopy and the fluorescence spectrum. The UV absorption spectrum of NCD presented obvious absorption peaks at around 350 nm, which was ascribable to the $\pi-\pi^*$ electronic transition of the C═C or C═O bond[39] (Figure S1). In addition, the fluorescence property was studied at different excitation wavelengths (Figure 3A). The highest emission peak was observed at 450 nm with an excitation wavelength of 350 nm. A redshift in the fluorescence emission spectrum was observed when the excitation wavelength varied in the range of 310−380 nm. Similar observations were reported in Baraa's study, suggesting that the redshift phenomenon may be attributed to a reduced bandgap caused by the presence of multiple emission centers or differences in particle morphology within the fluorophore.[40,41] Based on the experimental results, we opted for a fixed excitation wavelength of 350 nm for subsequent experiments. As the excitation wavelength varied from 310 to 380 nm, the emission peak wavelength was redshifted and the maximum intensity of the emission peak changed. The maximum emission wavelength of NCD was at 450 nm with an excitation of 350 nm. Therefore, an excitation wavelength of 350 nm was selected as a fixed excitation wavelength in the following research.

To achieve the optimum linear range and sensitivity, we investigated the fluorescence intensity of NCD under extreme pH conditions, various storage durations, different additive concentrations, varied reaction times, and diverse temperature conditions. The fluorescence spectrum of NCD is shown in Figure 3B. It indicated that the fluorescence intensity was unaffected by pH condition as the pH ranged from 6 to 9. However, under strong acidic or alkaline conditions, the fluorescence intensity of NCD significantly decreased. This phenomenon may be attributed to structural changes in the fluorophore itself in the strong acidic or alkaline environment.[42] In addition, the detection temperature and storage time of NCD did not affect the fluorescence intensity (Figures 4A,B, S2 and S3). The above results indicated that NCD prepared in our study exhibits a high level of stability. Furthermore, the fluorescence intensity of NCD varied with the concentrations (Figure 4C). To obtain the optimal detection time, the quenching experiments were performed with different reaction times (Figure 4D). The NCD could be quenched in 1 min and the quenching efficiency remained unchanged within 20 min. Thus, according to the results, the best detection condition was that the concentration of NCD was 1 mg/mL at 37 °C with pH value of 7.

3.3. Detection of NFT. To investigate the fluorescence quenching performance of NCD, the sensitivity experiment of NCD to NFT was studied under optimal conditions. As shown in Figure 5A, the fluorescence intensity of NCD sharply decreased with the addition of NFT and the fluorescence intensity was quenched gradually with increasing the concentration of antibiotics. To measure the residual NFT, the relationship further quantitatively between the fluorescence quenching efficiency of NCDs and the concentrations of NFT are exhibited in Figure 5B. Accordingly, the fluorescence quenching efficiency and concentration of NCD showed a good linear relationship in the range of 0.625−10 mg/mL with the linear correlation coefficient of 0.9915. The detection limit (LOD) was 0.0365 mg/mL based on the formula of $3\sigma/k$ (σ and k represent the standard deviation and slope of the curve, respectively). NCD displayed perfect sensitivity to NFT.

Selectivity also played a critical role in establishing the detection method because the actual samples usually contain many other antibiotics. The selectivity was investigated using different antibiotics, such as polymyxin, ampicillin enrofloxacin, cefpirome, gentamicin, and streptomycin. It can be seen from Figures S4 and S5 that the NFT demonstrated the most prominent fluorescence quenching effect on NCD compared with other antibiotics tested, while the fluorescence intensity of NCD did not significantly decrease with the introduction of other antibiotics. Moreover, NFT was added to the solution of NCD, which contained other antibiotics to appraise the selectivity of NCD for NFT (Figure 5C). The results indicated that other antibiotics had no influence on the detection of NFT. Therefore, according to the results, NCD obtained perfect specificity for NFT. Different methods from the literature were summarized and compared to the current method in terms of materials used, preparation method, linear range, limit of detection, recovery rate, and practical application (Table S1). The NCD not only had a short preparation time but also exhibited a low synthesis cost, making it suitable for large-scale production. Additionally, the NCD with high selectivity can rapidly detect the presence of NFT in less than 1 min. The proposed method, with the advantages of being rapid, cheap, and high selectivity, provided a novel approach for the detection of veterinary drug residue.

3.4. Quenching Mechanism. To elucidate the possible quenching mechanism, the fluorescence lifetimes of NCD and NCD/NFT mixtures were measured using a steady-state/lifetime spectrofluorometer. As shown in Figure 5D, the fluorescence lifetime of NCD/NFT mixture was 8.59 ns, which was almost unchanged from that of NCD (8.86 ns). These results confirmed that the quenching process was inner filter effect (IFE) or static quenching, ruling out dynamic quenching. To further verify the quenching mechanism, the UV−vis spectra of NFT and fluorescence spectrum of NCD are shown in Figure 5E. NFT had a maximum absorption band at 370 nm that obviously overlapped the excitation/emission spectrum of NCD. Moreover, the fluorescence intensity of NCD gradually decreased with the addition of NFT (Figure 5A). The observed fluorescence quenching of NCD by NFT may had resulted from IFE.[43−45] To exclude the static quenching, the absorption spectra of NCD, NFT and NCD/NFT mixture were examined (Figure S7A). The absorption curve of the NCD/NFT mixture was almost significantly different from those of the sum value of NCD and NFT. Therefore, the static quenching mechanism of NCD by NFT cannot be ruled out. Meanwhile, the UV absorption intensities of NCD increased with an increase of NFT (Figure S7B). It also indicated that the fluorescence quenching was static quenching. To sum up, the fluorescence quenching mechanism of NCD by NFT mainly resulted from IFE and static quenching.[46]

https://doi.org/10.1021/acsomega.3c09620
ACS Omega 2024, 9, 13183−13190

3.5. Detection of NFT in Real Samples. In order that verify the detection of NFT in actual samples, NFT was added to milk and meat samples, and the method was used for detection. As shown in Table 1, the recovery of NFT in samples was 94.00−108.00% and the relative standard deviation was 3.94−5.74% (n = 5). In preliminary experiments, we discovered that NCD can serve as fluorescence sensors for detecting antibiotic. To further investigate the detection capabilities of NCD in real samples, this experiment employed milk and meat supernatant solutions with varying concentrations of NFT as test liquids. In different concentrations of NFT solutions prepared with milk, the quenching effect on the fluorescence of NCD was observed as depicted in Figure S6A. The fluorescence intensity reached its maximum when the concentration of the NFT solution was 0.2 mg/mL. As the concentration increased, the degree of fluorescence quenching intensified. When the concentration of the NFT solution reached 0.4 mg/mL, the fluorescence intensity diminished, indicating the optimal fluorescence quenching effect. Similarly, in different concentrations of NFT solutions prepared with the meat supernatant, the quenching effect on the fluorescence of NCD followed a trend similar to that of the previous test liquid (Figure S6B). With an increase in the concentration of the test liquid, the detected fluorescence intensity decreased, indicating an enhanced quenching effect of NCD. The fluorescence method could be used for quickly and accurately detecting the NFT in real samples and possessed great value for practical applications.

Table 1. Determination of NFT in Real Samples

sample	added (mg/mL)	measured (mg/mL)	recovery rate (%)	RSD (%, n = 5)
milk	0.400	0.393	98.25	5.74
	0.300	0.311	103.67	4.89
	0.200	0.188	94.00	5.11
meat	0.400	0.411	102.75	3.94
	0.300	0.289	96.33	4.52
	0.200	0.216	108.00	4.63

4. CONCLUSIONS

In conclusion, NCD with high fluorescence retention and good stability were synthesized using citric acid and urea by a facile and eco-friendly one-step microwave method. TEM, XRD, FT-IR, and XPS analysis supported that the nitrogen element was successfully doped into the skeleton of carbon dots. The NCD displayed fluorescence property with the wavelength varied from 310 to 380 nm, and the maximum emission wavelength of NCD was 450 nm with an excitation of 350 nm. Besides, the fluorescence intensity was quenched gradually with increasing concentration of NFT and a satisfactory linear relationship between the fluorescence quenching efficiency and concentrations of NFT was obtained. In practical sample testing, as the concentration of NFT increased, a significant reduction in the fluorescence intensity of NCD was observed. It was indicated that NCD was qualitatively and quantitatively applied for detection NFT in milk and meat extract samples with a high recovery rate. Consequently, the detection method has potential application in the specific detection of NFT, offering a novel approach for veterinary drug residue detection.

ASSOCIATED CONTENT

Supporting Information

The Supporting Information is available free of charge at https://pubs.acs.org/doi/10.1021/acsomega.3c09620.

UV−vis spectrum of NCD, fluorescence spectra of NCD with different conditions; quenching of NCD in milk and meat supernatant; UV−vis spectrum of NFT, NCD, NCD/NFT mixture and the sum of NCDs and NFT absorbance values; the UV−vis spectrum of NFT mixed with NCD; and the determination of nitrofurantoin using different methods (PDF)

AUTHOR INFORMATION

Corresponding Authors

Hui Xia − *College of Chemistry & Environment, Southwest Minzu University, Chengdu 610041, China*; Email: ivyxiahui@swun.edu.cn

Lu Wang − *College of Animal and Veterinary Sciences, Southwest Minzu University, Chengdu, Sichuan 610041, China*; orcid.org/0000-0001-7590-2234; Email: luwangbest@163.com

Authors

Xing Zhao − *College of Animal and Veterinary Sciences, Southwest Minzu University, Chengdu, Sichuan 610041, China*

Shiwen Chen − *College of Animal and Veterinary Sciences, Southwest Minzu University, Chengdu, Sichuan 610041, China*

Yangyang Fan − *College of Animal and Veterinary Sciences, Southwest Minzu University, Chengdu, Sichuan 610041, China*

Xianglan Lei − *College of Animal and Veterinary Sciences, Southwest Minzu University, Chengdu, Sichuan 610041, China*

Yulin Li − *College of Animal and Veterinary Sciences, Southwest Minzu University, Chengdu, Sichuan 610041, China*

Tianxing Ji − *College of Animal and Veterinary Sciences, Southwest Minzu University, Chengdu, Sichuan 610041, China*

Complete contact information is available at: https://pubs.acs.org/10.1021/acsomega.3c09620

Author Contributions

[§]X.Z. and S.C. contributed equally to this work.

Notes

The authors declare no competing financial interest.

ACKNOWLEDGMENTS

This work was financially supported by Sichuan Science and Technology Program (2022JDRC0115) and Fundamental Research Funds for Central Universities, Southwest Minzu University (2022NYXXS037).

REFERENCES

(1) Le, V. V. H.; Rakonjac, J. Nitrofurans: Revival of an "old" drug class in the fight against antibiotic resistance. *PLoS Pathog.* **2021**, *17* (7), No. 1009663.

(2) Melekhin, A. O.; Tolmacheva, V. V.; Apyari, V. V.; Dmitrienko, S. G. Current trends in analytical strategies for the chromatographic

determination of nitrofuran metabolites in food samples. An update since 2012. *Journal of Chromatography. A* **2022**, *1685*, No. 463620.
(3) Jia, J.; Zhang, H.; Qu, J.; Wang, Y.; Xu, N. Immunosensor of Nitrofuran Antibiotics and Their Metabolites in Animal-Derived Foods: A Review. *Front Chem.* **2022**, *10*, No. 813666.
(4) Jang, H. M.; Yoo, S.; Choi, Y.-K.; Park, S.; Kan, E. Adsorption isotherm, kinetic modeling and mechanism of tetracycline on Pinus taeda-derived activated biochar. *Bioresour. Technol.* **2018**, *259*, 24−31.
(5) Liu, H.; Wei, Y.; Luo, J.; Li, T.; Wang, D.; Luo, S.; Crittenden, J. C. 3D hierarchical porous-structured biochar aerogel for rapid and efficient phenicol antibiotics removal from water. *Chemical Engineering Journal* **2019**, *368*, 639−648.
(6) Fan, W.; Gao, W.; Jiao, J.; Wang, D.; Fan, M. Highly sensitive SERS detection of residual nitrofurantoin and 1-amino-hydantoin in aquatic products and feeds. *Luminescence* **2022**, *37* (1), 82−88.
(7) Fernandes, G.; Salgado, H.; Santos, J. A critical review of HPLC-based analytical methods for quantification of Linezolid. *Crit. Rev. Anal. Chem.* **2020**, *50*, 196−211.
(8) Šlampová, A.; Kubáň, P. Electromembrane extraction - capillary zone electrophoresis for the quantitative determination of β-lactam antibiotics in milk samples. *J. Chromatogr A* **2023**, *1711*, No. 464455.
(9) Berska, J.; Bugajska, J.; Sztefko, K. A Liquid Chromatography-Tandem Mass Spectrometry Method for Simultaneously Determining Meropenem and Linezolid in Blood and Cerebrospinal Fluid. *Ann. Lab Med.* **2024**, *44* (2), 174−178.
(10) Zamora-Sequeira, R.; Starbird-Pérez, R.; Rojas-Carillo, O.; Vargas-Villalobos, S. What are the Main Sensor Methods for Quantifying Pesticides in Agricultural Activities? A Review. *Molecules (Basel, Switzerland)* **2019**, *24* (14), 2659.
(11) Fan, H.; Zhang, M.; Bhandari, B.; Yang, C.-H Food waste as a carbon source in carbon quantum dots technology and their applications in food safety detection. *Trends in Food Science & Technology* **2020**, *95*, 86−96.
(12) Chu, H.-W.; Unnikrishnan, B.; Anand, A.; Lin, Y.-W.; Huang, C.-C. Carbon quantum dots for the detection of antibiotics and pesticides. *Journal of Food and Drug Analysis* **2020**, *28* (4), 540−558.
(13) Fu, Y.; Liu, T.; Zhang, Z.; Li, H.; Li, W.; Huang, M. The crosstalk fluorescence spectroscopy analysis principle and an accurate fluorescence quantitative method for multi-composition fluorescence substances. *Spectrochim Acta A Mol. Biomol Spectrosc* **2022**, *280*, No. 121472.
(14) Xia, Z.; Li, Q. Application of Metronidazole detection by antibiotic ampicillin sodium based-carbon quantum dots. *International Journal of Environmental Analytical Chemistry* **2022**, *102* (16), 4178−4190.
(15) Yuan, A.; Lei, H.; Xi, F.; Liu, J.; Qin, L.; Chen, Z.; Dong, X. Graphene quantum dots decorated graphitic carbon nitride nanorods for photocatalytic removal of antibiotics. *J. Colloid Interface Sci.* **2019**, *548*, 56−65.
(16) Fu, Y.; Zhao, S.; Wu, S.; Huang, L.; Xu, T.; Xing, X.; Lan, M.; Song, X. A carbon dots-based fluorescent probe for turn-on sensing of ampicillin. *Dyes Pigm.* **2020**, *172*, No. 107846.
(17) Li, W.-K.; Feng, J.-T.; Ma, Z.-Q. Nitrogen, sulfur, boron and flavonoid moiety co-incorporated carbon dots for sensitive fluorescence detection of pesticides. *Carbon* **2020**, *161*, 685−693.
(18) Hu, C.; Su, T.-R.; Lin, T.-J.; Chang, C.-W.; Tung, K.-L. Yellowish and blue luminescent graphene oxide quantum dots prepared via a microwave-assisted hydrothermal route using H_2O_2 and $KMnO_4$ as oxidizing agents. *New J. Chem.* **2018**, *42*, 3999−4007.
(19) Han, Z.; Zhang, H.; He, L.; Pan, S.; Liu, H.; Hu, X. One-pot hydrothermal synthesis of nitrogen and sulfur co-doped carbon dots and their application for sensitive detection of curcumin and temperature. *Microchemical Journal* **2019**, *146*, 300−308.
(20) Tan, Q.; Zhang, R.; Zhang, G.; Liu, X.; Qu, F.; Lu, L. Embedding carbon dots and gold nanoclusters in metal-organic frameworks for ratiometric fluorescence detection of Cu2+. *Anal. Bioanal. Chem.* **2020**, *412* (6), 1317−1324.
(21) Yan, F.; Jiang, Y.; Sun, X.; Bai, Z.; Zhang, Y.; Zhou, X. Surface modification and chemical functionalization of carbon dots: a review. *Microchim. Acta* **2018**, *185* (9), 424.
(22) Ghosal, K.; Ghosh, A. Carbon dots: The next generation platform for biomedical applications. *Materials Science & Engineering. C, Materials for Biological Applications* **2019**, *96*, 887−903.
(23) Chen, M. C.; Chen, D. G.; Chou, P. T. Fluorescent Chromophores Containing the Nitro Group: Relatively Unexplored Emissive Properties. *ChemPlusChem.* **2021**, *86* (1), 11−27.
(24) Ma, Q.; Zhang, Z.; Yu, Z. Synthesis of carbon quantum dots and zinc oxide nanosheets by pyrolysis of novel metal−organic framework compounds. *J. Alloys Compd.* **2015**, *642*, 148−152.
(25) Qiao, L. n.; Qian, S.; Wang, Y.; Yan, S.; Lin, H. Carbon-Dots-Based Lab-On-a-Nanoparticle Approach for the Detection and Differentiation of Antibiotics. *Chemistry − A. European Journal* **2018**, *24* (18), 4703−4709.
(26) Yang, L.; Zhao, H.; Liu, N.; Wang, W. A target analyte induced fluorescence band shift of piperazine modified carbon quantum dots: a specific visual detection method for oxytetracycline. *Chem. Commun.* **2019**, *55* (82), 12364−12367.
(27) Qi, H.; Teng, M.; Liu, M.; Liu, S.; Li, J.; Yu, H.; Teng, C.; Huang, Z.; Liu, H.; Shao, Q.; et al. Biomass-derived nitrogen-doped carbon quantum dots: highly selective fluorescent probe for detecting Fe3+ ions and tetracyclines. *J. Colloid Interface Sci.* **2019**, *539*, 332−341.
(28) Kumar, A.; Kuang, Y.; Liang, Z.; Sun, X. M. Microwave chemistry, recent advancements, and eco-friendly microwave-assisted synthesis of nanoarchitectures and their applications: a review. *Mater. Today Nano* **2020**, *11*, No. 100076.
(29) Lin, H.; Huang, J.; Ding, L. Preparation of Carbon Dots with High-Fluorescence Quantum Yield and Their Application in Dopamine Fluorescence Probe and Cellular Imaging. *J. Nanomater.* **2019**, *2019*, 1−9.
(30) Khataee, A.; Jalili, R.; Dastborhan, M.; Karimi, A.; Ebadi Fard Azar, A. Ratiometric visual detection of tetracycline residues in milk by framework-enhanced fluorescence of gold and copper nanoclusters. *Spectrochim. Acta, Part A* **2020**, *242*, No. 118715.
(31) Zhang, H.; Zhou, Q.; Han, X.; Li, M.; Yuan, J.; Wei, R.; Zhang, X.; Wu, M.; Zhao, W. Nitrogen-doped carbon dots derived from hawthorn for the rapid determination of chlortetracycline in pork samples. *Spectrochimica Acta. Part A, Molecular and Biomolecular Spectroscopy* **2021**, *255*, No. 119736.
(32) John, B. K.; Abraham, T.; Mathew, B. A Review on Characterization Techniques for Carbon Quantum Dots and Their Applications in Agrochemical Residue Detection. *J. Fluoresc.* **2022**, *32* (2), 449−471.
(33) Lee, J.; Kim, N.; Shin, D. Y.; Park, H.-Y.; Lee, S.-S.; Kwon, S.; Lim, D.-H.; Bong, K.; Son, J.; Kim, J. Nitrogen-doped graphene-wrapped iron nanofragments for high-performance oxygen reduction electrocatalysts. *J. Nanopart. Res.* **2017**, *19*, 98.
(34) Wang, Q.; Zhang, C.; Shen, G.; Liu, H.; Fu, H.; Cui, D. Fluorescent carbon dots as an efficient siRNA nanocarrier for its interference therapy in gastric cancer cells. *J. Nanobiotechnol.* **2014**, *12*, 58.
(35) Li, L.; Zhang, H.; Cheng, A.; Zhong, W.; Li, Z. Recent discovery of a multifunctional metallo-organic precursor for fabricating Co3O4/N-doped porous carbon by one-step in situ pyrolysis as an anode material for Li-ion batteries. *J. Mater. Sci.* **2021**, *56*, 1590−1599.
(36) Nguyen, T. N.; Le, P. A.; Phung, V. B. T. Facile Green Synthesis of Carbon Quantum Dots and Biomass-Derived Activated Carbon from Banana Peels: Synthesis and Investigation. *Biomass Conversion and Biorefinery* **2022**, *12*, 2407−2416.
(37) Wang, X.; Yang, P.; Feng, Q.; Meng, T.; Wei, J.; Xu, C.; Han, J. Green Preparation of Fluorescent Carbon Quantum Dots from Cyanobacteria for Biological Imaging. *Polymers* **2019**, *11*, 616.
(38) Ma, X.; Li, S.; Hessel, V.; Lin, L.; Meskers, S.; Gallucci, F. Synthesis of luminescent carbon quantum dots by microplasma process. *Chem. Eng. Process.* **2019**, *140*, 29−35.

https://doi.org/10.1021/acsomega.3c09620
ACS Omega 2024, 9, 13183−13190

(39) Zhu, S.; Wang, K.; Hu, J.; Liu, R.; Zhu, H. Nitrogen and sulphur co-doped carbon quantum dots and their optical power limiting properties. *Mater. Adv.* **2020**, *1* (9), 3176−3181.
(40) Al-Hashimi, B. R.; Omer, K. M.; Rahman, H. S.; Othman, H. H. Inner filter effect as a sensitive sensing platform for detection of nitrofurantoin using luminescent drug-based carbon nanodots. *Spectrochim Acta A Mol. Biomol Spectrosc* **2021**, *244*, No. 118835.
(41) Lai, S.; Jin, Y.; Shi, L.; Zhou, R.; Zhou, Y.; An, D. Mechanisms behind excitation- and concentration-dependent multicolor photoluminescence in graphene quantum dots. *Nanoscale* **2020**, *12* (2), 591−601.
(42) Yang, Y. Z.; Xiao, N.; Liu, S. G.; Han, L.; Li, N. B.; Luo, H. Q. pH-induced aggregation of hydrophilic carbon dots for fluorescence detection of acidic amino acid and intracellular pH imaging. *Mater. Sci. Eng. C Mater. Biol. Appl.* **2020**, *108*, No. 110401.
(43) Lin, M.; Zou, H. Y.; Yang, T.; Liu, Z. X.; Liu, H.; Huang, C. Z. An inner filter effect based sensor of tetracycline hydrochloride as developed by loading photoluminescent carbon nanodots in the electrospun nanofibers. *Nanoscale* **2016**, *8* (5), 2999−3007.
(44) Fan, H.; Xiang, G. Q.; Wang, Y.; Zhang, H.; Ning, K.; Duan, J.; He, L.; Jiang, X.; Zhao, W. Manganese-doped carbon quantum dots-based fluorescent probe for selective and sensitive sensing of 2,4,6-trinitrophenol via an inner filtering effect. *Spectrochim Acta A Mol. Biomol Spectrosc* **2018**, *205*, 221−226.
(45) Su, K.; Xiang, G.; Jin, X.; Wang, X.; Jiang, X.; He, L.; Zhao, W.; Sun, Y.; Cui, C. Gram-scale synthesis of nitrogen-doped carbon dots from locusts for selective determination of sunset yellow in food samples. *Luminescence* **2022**, *37* (1), 118−126.
(46) Long, C. C.; Jiang, Z. X.; Shangguan, J. F.; Qing, T. P.; Zhang, P.; Feng, B. Applications of carbon dots in environmental pollution control: A review. *Chemical Engineering Journal* **2021**, *406*, No. 126848.

https://doi.org/10.1021/acsomega.3c09620
ACS Omega 2024, 9, 13183−13190